CALIFORNIA INSTITUTE OF TECHNOLOGY

EARTHQUAKE ENGINEERING RESEARCH LABORATORY

AMBIENT VIBRATION SURVEYS OF THREE STEEL-FRAME BUILDINGS STRONGLY SHAKEN BY THE 1994 NORTHRIDGE EARTHQUAKE

BY

JAMES L. BECK, B. SCOTT MAY,
DAVID C. POLIDORI, AND MICHAEL W. VANIK

REPORT NO. EERL 95-06

A REPORT ON RESEARCH CONDUCTED UNDER A SUBCONTRACT FROM SAC JOINT VENTURE

FUNDED BY
THE FEDERAL EMERGENCY MANAGEMENT AGENCY (FEMA)

PASADENA, CALIFORNIA
DECEMBER 1995

Ambient Vibration Surveys of Three Steel-Frame Buildings Strongly Shaken by the 1994 Northridge Earthquake

by

James L. Beck, B. Scott May, David C. Polidori and Michael W. Vanik

Report No. EERL 95-06

A Report on Research Conducted Under a Subcontract
from SAC Joint Venture

SAC Joint Venture: A partnership of
the Structural Engineers Association,
the Applied Technology Council, and
the California Universities for Research in
Earthquake Engineering

Funded by
the Federal Emergency Management Agency (FEMA)

California Institute of Technology
Pasadena, California
December 1995

This report covers research conducted under a subcontract with the SAC Joint Venture which was funded by the Federal Emergency Management Agency (FEMA).

The SAC Joint Venture entered into a contract with the Federal Emergency Management Agency (FEMA) to furnish all professional, technical and clerical personnel, services, materials, equipment and facilities to conduct a "Program to Reduce Earthquake Hazards in Steel Moment Frame Structures." This publication reports on the research conducted under a subcontract between this Joint Venture and Professor James L. Beck of the California Institute of Technology.

Ambient vibration surveys of three steel-frame buildings strongly shaken by the 1994 Northridge Earthquake (SAC Project Sub-Task 3.2)

James L. Beck
B. Scott May
David C. Polidori
Michael W. Vanik
CALIFORNIA INSTITUTE OF TECHNOLOGY

SUMMARY

Ambient vibration surveys (AVS) can be used efficiently, cheaply and unobtrusively to identify the small-amplitude periods and modeshapes of lower modes of vibration of structures. Under Task 3.2 of Phase I of the SAC Steel Building Program, AVS were performed on three steel-frame buildings which experienced strong shaking during the January 17, 1994 Northridge earthquake.

The primary objective of this study was to identify the small-amplitude modal parameters of the buildings for assessment of the analytical models constructed by others under SAC Task 3.1. A preliminary comparison of the modal periods obtained from the AVS with those calculated from the analytical models is presented. Although the periods identified from the AVS were considerably shorter than the model periods, the ratios of the identified to model periods for each mode were quite similar. The differences in periods are thought to be primarily because the analytical models treat only the structural frame, ignoring the stiffness of nonstructural components such as architectural partitions and building cladding.

This study also serves as a first step in the testing of proposed structural health monitoring methodologies. Since one of the tested steel-frame buildings was damaged and has not yet been repaired, its data represent an "after" damage state. The tests on this steel-frame building can be followed later by an AVS if the structure is repaired. These "before" and "after" AVS results would provide valuable data to test proposed global structural health monitoring methodologies whose goal is to detect, locate and assess damage by monitoring ambient vibrations. A successful structural health monitoring method would allow "hidden" damage to be detected almost immediately rather than weeks after an earthquake.

INTRODUCTION

CONTEXT OF SAC JOINT-VENTURE TASK 3.2

The intent of Task 3 of the SAC Joint Venture is to perform detailed assessment of the performance of selected steel-frame buildings which were damaged during the January 17, 1994 Northridge Earthquake. These investigations focus on identifying the specific causes of the failures, assessment of the accuracy of current analytical models used to predict where the failure may occur during strong shaking, and identifying conditions under which more severe, life threatening damage might occur. Analytical models of selected buildings which were damaged during the Northridge Earthquake are being constructed under Task 3.1, while Task 3.2, which is the subject of this report, involves field testing of these buildings in an effort to assess the accuracy of the models.

GOALS

Our objective under Task 3.2 is to perform ambient vibration tests on selected steel-frame buildings to obtain their small-amplitude "elastic" dynamic characteristics for assessment of the dynamic models constructed by others under Task 3.1. For buildings damaged and not yet repaired, the dynamic characteristics can also be compared with those determined in later tests when the buildings have been repaired so that the extent of changes produced by the failed connections can be determined. Ambient vibration tests can be used to efficiently determine the small-amplitude periods and modeshapes for the lower modes of vibration of a building. These modal parameters can then be compared with those computed from an analytical model. We have recently developed an efficient time-domain method for estimating modal parameters from ambient vibration data. The effectiveness of this method was demonstrated earlier by performing ambient vibration tests on the nine-story Millikan Library at Caltech (Beck et al., 1994a).

Because measurement of ambient vibrations, either in special tests or by continuous monitoring, can be done cheaply and in a relatively unobtrusive way, determining whether these data can be used to detect and locate failed connections or other localized damage is of much interest. We are currently performing research in this area since it has the potential to provide a cost-effective global non-destructive evaluation (NDE) method for rapidly assessing the integrity of structures immediately following an earthquake. The opportunity to test steel buildings with different degrees of damage before they are repaired will allow a valuable database to be constructed which can be used to assess this structural health monitoring methodology in follow-on projects. The idea here is to do "reverse sequence" damage detection tests; those done now provide "post-damage" data while those done after the connections have been repaired will be viewed as providing "pre-damage" data.

CONTENTS OF THIS DOCUMENT

In the next section, the methodology for the time-domain extraction of modal information from ambient vibration data is developed. This method is based on the theoretical correlation function of the response, and makes use of the efficient modal-identification algorithm MODE-ID to determine the modal parameters.

The third section describes both the analysis procedure, which is based on the theory of the preceding section, and the experimental setup for the ambient vibration surveys. The analysis procedure uses MODE-ID to identify the modal parameters from the sample correlation function by treating the latter as a pseudo-free-vibration response. For the field testing, the ambient vibration response is recorded at several locations in a building in order to capture all its lower modes and the corresponding modeshapes.

The fourth section describes the ambient vibration survey (AVS) performed on two new steel-frame buildings located on the campus of California State University, Northridge. The four-story structure had been repaired after suffering numerous connection failures during the Northridge earthquake. The two-story building was undamaged. The modal periods obtained from the AVS are compared with those from the structural analysis performed by H. Krawinkler at Stanford University (see the Task 3.1 Report).

The fifth section describes the AVS performed on an 11-story steel-frame structure in West LA (referred to as SAC Building 6 of Task 3 herein). This structure has not been repaired. The identified modal periods are compared with those from the analysis performed by F. Naeim of John A. Martin & Associates (see the Task 3.1 Report).

The final section presents the conclusions drawn from the ambient vibration surveys and recommends some future studies on steel-frame buildings.

MODAL-IDENTIFICATION METHODOLOGY

INTRODUCTION

Extracting modal parameters from naturally occurring small-amplitude ("ambient") vibrations in a structure is a challenging problem because of the poor signal-to-noise ratios and the fact that the excitation forces are not known. The modal parameter estimation is usually performed in the frequency domain, but we describe here an efficient time-domain method which can be mostly automated (Beck et al., 1994a).

Under stationary Gaussian white-noise excitation, the theoretical correlation function for the response of a classically-damped linear system can be shown to be the sum of decaying sinusoids (James et al., 1992). The frequencies, decay ratios, and relative amplitudes of these sinusoids correspond to the natural frequencies, damping ratios, and modeshapes of the linear system. These decaying sinusoids are identical to the free-vibration response of the same linear system with appropriately chosen initial conditions. This allows the use of the efficient modal-identification algorithm MODE-ID (Beck, 1978) for extracting the modal parameters. The correlation function derivation is included in the next section. Following this, the MODE-ID program is described.

CORRELATION FUNCTION

Consider the system of n equations

$$M\ddot{x} + C\dot{x} + Kx = f(t) \tag{1}$$

where $x, f \in \mathbb{R}^n$ represent the displacement and the (random) excitation, respectively, and $M, C, K \in \mathbb{R}^{n\times n}$, are the mass, damping, and stiffness matrices. The correlation between two weakly-stationary signals, $x_i(t)$ and $x_j(t)$, is defined by

$$R_{x_i x_j}(T) \triangleq \mathrm{E}\left[x_i(t)x_j(t+T)\right]. \tag{2}$$

Under the assumptions of Gaussian white-noise input and a stable system exhibiting classical normal modes, the correlation function can be shown to consist of the sums of decaying sinusoids whose parameters correspond to the frequency, damping, and modeshape components of the system. This derivation follows below.

The necessary and sufficient conditions for the existence of classical normal modes are that the matrices $M^{-1}C$ and $M^{-1}K$ commute, i.e. $CM^{-1}K = KM^{-1}C$ (Caughey and O'Kelly, 1965). A non-singular matrix Φ can then be found such that $y = \Phi^{-1}x$ and

$$\Phi^T M \Phi = I \tag{3}$$

$$\Phi^T C \Phi = \Theta = \mathrm{diag}(2\zeta_r\omega_r) \tag{4}$$

$$\Phi^T K \Phi = \Lambda = \mathrm{diag}(\omega_r^2) \tag{5}$$

Equation 1 may now be rewritten in terms of the modal coordinates,

$$I\ddot{y} + \Theta\dot{y} + \Lambda y = \Phi^T f(t). \tag{6}$$

The equation of motion for the r^{th} modal coordinate $y_r(t)$ is

$$\ddot{y}_r + 2\zeta_r\omega_r\dot{y}_r + \omega_r^2 y_r = \sum_{i=1}^{N} \phi_i^{(r)} f_i(t) \tag{7}$$

where $\phi_i^{(r)}$ is the component of the r^{th} eigenvector at the i^{th} nodal point, and $f_i(t)$ is the excitation at that location.

Since the system is stable, the response of the r^{th} modal coordinate is

$$y_r(t) = \int_{-\infty}^{t} h_r(t-\eta) \sum_{i=1}^{N} \phi_i^{(r)} f_i(\eta) d\eta \tag{8}$$

where $h_r(t)$ is the impulse response function,

$$h_r(t) = \frac{1}{\bar{\omega}_r} \exp\left[-\zeta_r\omega_r t\right] \sin \bar{\omega}_r t \tag{9}$$

and $\bar{\omega}_r = \omega_r\sqrt{1-\zeta^2}$ is the damped natural frequency. Now, let $\tau = t-\eta$ and change variables in the above integral (Equation 8),

$$y_r(t) = \int_0^{\infty} h_r(\tau) \sum_{i=1}^{N} \phi_i^{(r)} f_i(t-\tau) d\tau. \tag{10}$$

The correlation function in terms of the modal coordinates is given by

$$R_{y_r y_s}(T) = \mathrm{E}\left[y_r(t) y_s(t+T)\right] \tag{11}$$

$$= \int_0^{\infty}\int_0^{\infty} h_r(\tau) h_s(\eta) \mathrm{E}\left[\sum_{i,j=1}^{N} \phi_i^{(r)}\phi_j^{(s)} f_i(t-\tau) f_j(t+T-\eta)\right] d\tau d\eta, \tag{12}$$

Since the excitation $f(t)$ is white,

$$\mathrm{E}\left[f_i(t-\tau) f_j(t+T-\eta)\right] = A_{ij}\delta(T+\tau-\eta), \tag{13}$$

and

$$R_{y_r y_s}(T) = \left(\int_0^{\infty} h_r(\tau) h_s(T+\tau) d\tau\right)\left(\sum_{i,j=1}^{N} \phi_i^{(r)}\phi_j^{(s)} A_{ij}\right). \tag{14}$$

Note that the integral depends only on the modal parameters ζ_r, ζ_s, ω_r, and ω_s, and can be evaluated analytically to obtain an expression of the form

$$\int_0^{\infty} h_r(\tau) h_s(T+\tau) d\tau = D_{rs}(\zeta_r, \omega_r, \zeta_s, \omega_s) \exp\left[-\zeta_s\omega_s T\right] \sin\left(\bar{\omega}_s T + \theta_{rs}^{(D)}\right), \tag{15}$$

where "D" is meant to denote "displacement." Transforming back to the nodal coordinates ($x_i = \sum_{r=1}^{N} \phi_i^{(r)} y_r$), the correlation function between nodes i and j is

$$R_{x_i x_j}(T) = \sum_{r,s=1}^{N} \phi_i^{(r)} \phi_j^{(s)} \left(\sum_{k,l=1}^{N} \phi_k^{(r)} \phi_l^{(s)} A_{kl} \right) D_{rs} \exp\left[-\zeta_s \omega_s T\right] \sin\left(\bar{\omega}_s T + \theta_{rs}^{(D)}\right). \tag{16}$$

After rearranging the summations in the above equation and making substitutions to simplify the expressions,

$$R_{x_i x_j}(T) = \sum_{s=1}^{N} \phi_i^{(s)} B_j^{(s)} \exp\left[-\zeta_s \omega_s T\right] \sin\left(\bar{\omega}_s T + \gamma_j^{(s)}\right), \tag{17}$$

where $B_j^{(s)}$ and $\gamma_j^{(s)}$ are constants resulting from the sum over r. Hence, the s^{th} mode of the correlation between the i^{th} and j^{th} outputs has a modeshape component at node i of $\phi_i^{(s)}$, a natural frequency ω_s and a damping ratio ζ_s. The constants $B_j^{(s)}$ and $\gamma_j^{(s)}$ depend only on the mode number s and node j. Therefore, by choosing a reference channel x_j and computing the correlation of all the other signals with this channel (i.e. $R_{x_1 x_j}, R_{x_2 x_j}, \ldots$), the modeshape components $\phi_i^{(s)}$ can be identified.

Similarly, the correlation of the velocities or the accelerations can be found. The procedure is the same as above for the displacement correlation function, except the derivatives of the impulse response functions are used. Different coefficients will be obtained when the following integral is evaluated to obtain the expression for the correlations of the velocities,

$$\int_0^\infty h_r(\tau) h_s(T+\tau) d\tau = V_{rs}(\zeta_r, \omega_r, \zeta_s, \omega_s) \exp\left[-\zeta_s \omega_s T\right] \sin\left(\bar{\omega}_s T + \theta_{rs}^{(V)}\right), \tag{18}$$

(c.f. Equation 15) using "V" to denote "velocity" and where

$$\dot{h}_r(t) = \exp\left[-\zeta_r \omega_r t\right] \left(\cos \bar{\omega}_r T - \frac{\zeta_r}{\sqrt{1-\zeta_r^2}} \sin \bar{\omega}_r T \right). \tag{19}$$

So, the velocity correlation function is

$$R_{\dot{x}_i \dot{x}_j}(T) = \sum_{r,s=1}^{N} \phi_i^{(r)} \phi_j^{(s)} \left(\sum_{k,l=1}^{N} \phi_k^{(r)} \phi_l^{(s)} A_{kl} \right) V_{rs} \exp\left[-\zeta_s \omega_s T\right] \sin\left[\bar{\omega}_s T + \theta_{rs}^{(V)}\right]. \tag{20}$$

By summing over r, this can be cast in the same form as Equation 17.

The acceleration correlation function can be derived from the equation of motion (Equation 1) and the two above correlation functions. Letting R_{XX} denote the matrix of correlation functions with components $(R_{XX})_{ij} = R_{x_i x_j}$, this relation can be expressed as

$$R_{\ddot{X}\ddot{X}}(T) = -M^{-1} C R_{\dot{X}\dot{X}}(T) - M^{-1} K R_{XX}(T) + M^{-1} R_{FF}(T) \tag{21}$$

where

$$R_{FF}(T) = \left[R_{f_i f_j}\right] = [A_{ij}]\,\delta(T). \tag{22}$$

Note then that the correlation of the accelerations is unbounded for $T = 0$, but is finite for all other T. Again, other than the $\delta(T)$ term, this function will reduce to a sum of decaying sinusoids as in Equation 17.

It can be shown that $R_{\dot{x}_i\dot{x}_j} \sim \omega_s^2 R_{x_i x_j}$ and $R_{\ddot{x}_i\ddot{x}_j} \sim \omega_s^4 R_{x_i x_j}$, so the higher-frequency modes receive a relatively larger weight for velocity or acceleration correlations. This is important, since typically the contribution of the higher modes to the response is small and hence they are difficult to identify in the presence of noise. Therefore, for larger contributions from the higher modes, velocity or acceleration measurements are more desirable than displacements. The ambient vibration surveys performed for this report used velocity measurements.

MODE-ID

MODE-ID is a time-domain modal identification program (Beck, 1978) which extracts the natural frequencies, damping ratios, and modeshape components of the linear model with classical normal modes that best fits the measured data in a least squares sense. The cost function, or measure-of-fit, is defined by

$$J(\psi) \triangleq \sum_{i=1}^{N} \|y(i\Delta t) - q(i\Delta t, f, \psi)\|^2 \tag{23}$$

where ψ is the vector of modal parameters, $y, q \in \mathbb{R}^{N_0 \times N}$ are the measured and model responses, N_0 is the number of output channels, f is the measured input, N is the number of sampled data points, and $\|\cdot\|$ is the Euclidean norm on $\mathbb{R}^{N_0}$. The model response, q, is calculated from the model with modal parameters ψ using the given inputs f. In the procedure, J is minimized with respect to ψ using a "modal-sweep" method, which is a combination of successive relaxation and a modified method of steepest descent. Previous studies (Beck and Beck, 1985) have shown that this approach is better in both accuracy and stability than a straight-forward transfer function approach. Also, within a Bayesian probability framework, the modal parameters estimated by MODE-ID can be viewed as the most probable values based on the given data (Beck, 1989).

Previously, MODE-ID has been applied to modal identification from measured seismic or forced response of high-rise buildings (Beck and Jennings, 1980; Nisar et al., 1992), a highway overpass (Werner et al., 1987), an off-shore oil platform (Mason et al., 1989), and other structures. Recently, MODE-ID has also been applied to modal identification from ambient vibrations on a 9-story reinforced-concrete building (Beck et al., 1994a), using the methodology described in this section.

ANALYSIS PROCEDURE AND EXPERIMENTAL SET-UP

ANALYSIS PROCEDURE

As was shown in the previous section, the theoretical correlation function is composed of sums of decaying sinusoids, closely resembling a free-vibration decay. MODE-ID efficiently extracts modal information from free-vibration response data, so the correlated signals are treated as such and processed using MODE-ID. When the output signals are correlated against the output from a common reference channel (x_j in Equation 17), the frequencies, damping ratios, and modeshape components are identified. The $B_j^{(s)}$'s and $\gamma_j^{(s)}$'s are related to the identified initial conditions for each mode at output j (the reference channel), and are of little interest in this study.

The analysis procedure begins with computing the sample correlation function from the vibration data. The velocity output from each of the 6 channels of data (digitized output from a Ranger seismometer, sampled at 500 Hz to avoid aliasing) are correlated against one common data channel. When performing experiments using a variety of sensor locations (to obtain more modeshape components), this sensor must remain in the same location so all the records can be correlated against its output. Hence, the data from this reference channel must be reliable and contain as much modal information as possible, since the sample correlations depend largely on the response of this channel. The reference location should be on the roof or top floor, to ensure that it is not located at a nodal point of one of the modes to be identified. A drawback to the roof or top floor location is that the amplitude of the fundamental mode dominates the channel's response, sometimes making identification of the higher modes difficult after the correlation function is computed. The sensor should also be isolated as much as possible from mechanical equipment such as exhaust fans or air conditioning, since the local vibrations caused by their operation may be large relative to the ambient response.

For records of finite duration it is well known (Bendat and Piersol, 1980) that the sample correlation gives an accurate approximation to the theoretical correlation for time lags less than one-tenth the duration of the signal. In order to obtain accurate modal parameter estimates from MODE-ID, the correlation signal should contain at least ten fundamental periods of the structure. To satisfy both of these requirements, for all three buildings tested, data was recorded for 180 seconds and the first 15 seconds of the sample correlations were used in MODE-ID.

The most efficient method to compute the sample correlation is to apply the Fast Fourier Transform (FFT) to the vibration data, square the amplitude of each complex transform value to obtain the power spectra, and then take the inverse FFT. The resulting signal is then low-pass filtered to reduce electrical noise and resampled at a lower rate to reduce the number of data points. For this analysis, a 10^{th}-order Tchebyshev filter with cut-off frequency

of 22.5 Hz is used for the filtering and the data is resampled at 125 Hz. The cut-off frequency of 22.5 Hz was chosen because the power spectra of the measured signals were small beyond this frequency except at a few isolated frequencies. These contributions were attributed to the electrical noise from the power supply and the local vibrations of the building's mechanical equipment.

Once the sample correlation function is obtained, the second step in the analysis is to run MODE-ID on the correlated signals to identify the modal parameters. MODE-ID requires a set of initial guesses for the frequency, damping, and modeshape components. The convergence of the algorithm is most sensitive to the initial guesses for the frequencies, which can easily be estimated by examining the power spectrum.

The final step in the analysis involves post-processing to visualize the modeshapes. The resulting pictures help determine the motion (e.g. 1^{st} north-south) of the identified modes.

EXPERIMENTAL SETUP

For the ambient vibration surveys, a 16-bit digital data acquisition system is used to measure the response of the buildings. The end-to-end system consists of 6 Kinemetrics Ranger Seismometers, two four-channel signal amplifiers, the 16-bit IOTech Daqbook 200 data acquisition system for analog-to-digital conversion, and a Zenith Z-Star laptop computer on which to store the digitized data. The laptop can also be used to analyze short data records at the site.

For each test, the signal amplifiers, Daqbook, and laptop computer are set up at a convenient location, typically close to a power supply and a stairwell. The stairwell facilitates access to the rest of the building with the seismometer cables. The seismometers are connected to long cables and placed in various locations throughout the structure to obtain modeshape information. Two checks are made prior to acquiring the data. First, the output from each channel is viewed with an oscilloscope to make sure the seismometers are registering a signal. Then, a short ($\approx$15 seconds) data sample is taken (at 500 Hz) and the Fourier amplitude spectrum is examined to ensure that the instruments are functioning properly. Once the checks are completed, three or four sets of data are recorded for 3 minutes at 500 Hz for each instrument configuration. The data from these longer data runs are then analyzed at Caltech. At some point in the field test, the seismometers are all placed at the same location to obtain the calibration factors for their outputs.

CSUN BUILDINGS

The goal of the first tests of the project was to measure the ambient vibrations in a new four-story steel-frame building, located on the campus of California State University, Northridge. The building was heavily damaged during the 1994 Northridge Earthquake (over 60% of the moment connections for north-south frames failed) but had been repaired by the time of our testing. Ambient vibration measurements were also taken in the adjacent two-story steel-frame building because of the interest expressed by H. Krawinkler and C. Thiel, who were analyzing both buildings. The adjacent structure's connections were of identical design and were constructed at the same time as those of the four-story building, but were undamaged by the earthquake.

The tests were performed from 7:30 P.M. to 1:30 A.M. on February 17-18, beginning about two hours after dark, so temperatures were relatively stable. The evening was breezy with moderate gusting throughout the testing. Typical windspeeds were estimated to be 10-15 mph at roof level, although no anemometer records were kept. The building was unoccupied except for our testing crew.

BUILDING DESCRIPTIONS

A typical floor plan for the four-story steel-frame building is included in **Figure 1-1**. The structure is seismically isolated from the two adjacent structures, a two-story steel-frame building to the north and another four-story structure to the east. The four-story building tested is rectangular in shape, approximately 63 ft. by 120 ft., with the longer direction running east-west. A stairway in the northwest corner of the building provided access for the seismometer cables. The building has no basement.

The adjacent two-story building which was also tested is quite long ($\approx$200 ft.) in the north-south direction, and narrow in the east-west ($\approx$50 ft.). This building also has no basement.

H. Krawinkler and C. Thiel provided a table of model periods for the four story building from their Task 3.1 study (see **Table 1-1** and **Table 1-3**).

SENSOR CONFIGURATIONS

Three sets of seismometer configurations were used to measure vibrations in the two buildings. For the first set of tests, the sensors were located on each floor of the four-story building to determine the modeshapes in each direction. The six Ranger seismometers were initially all aligned facing south. Rangers 1, 2, 4, and 5 were on the 2nd, 3rd, 4th, and roof levels respectively, and were located at the '$\times$' in the northwest corner of **Figure 1-1**. Rangers 3 and 6 were located on the 3rd and roof levels on the '$\times$' located in the southeast corner. The

exhaust fans and air-conditioning equipment on the roof were quite noisy, and Ranger 6 on the roof was located fairly close (<10 ft.) to an exhaust fan (Ranger 5 was much further from any mechanical equipment). With the sensors all facing south, four sets of data were recorded at a sampling rate of 500 Hz, the first for 90 seconds and the last three for 180 seconds. The seismometers were then rotated to face east, and four more data sets were recorded for 180 seconds each. The torsional modes can be distinguished from translational ones by noting that the modeshape components for the torsional modes at Rangers 2 and 3 (or 5 and 6) have opposite signs in torsion, but the same sign for pure flexural modes.

The second set of tests were done to determine the rocking and torsional motion of the four-story building at its foundation, so five seismometers were placed at ground level and one (Ranger 4) was left as a reference on the 4th floor. Of the five on the ground level, Ranger 1 was facing east and placed in the northwest corner of the building, Ranger 2 was facing up at the north side of the central north-south column line (line C in **Figure 1-1**), Ranger 3 was facing south and located in the northeast corner, Ranger 5 was facing south in the building's northwest corner, and Ranger 6 was facing up at the south side of the central north-south column line. Three data sets were recorded for 180 seconds at 500 Hz.

The third and final set of tests measured the vibrations of the two-story structure. Three seismometers were placed on the roof, and three on the second floor as shown in **Figure 1-2**. Again, three sets of data were recorded for 180 seconds at 500 Hz.

DATA PROCESSING

The majority of the data processing was performed at Caltech using the scheme discussed in the preceding section. One of the seismometers (Ranger 3 at the southeast corner of the third floor) was not functioning during the north-south tests, but was fine for the other tests. In addition, the exhaust fan close to Ranger 6 on the roof dominated the response from that channel, making extracting modal information from it difficult. Ranger 2, located in the northwest corner of the 3^{rd} floor, was chosen as the reference over the preferred roof or top floor sensors, since the modeshape component of the second north-south flexural modes was quite small at the fourth floor and the roof location was too noisy. By comparing the results from the different runs, the best estimates of the modal parameters were made.

Although the modal information was difficult to extract from the two-story building, some results are presented in the next section. The data from the seismometers located on the roof were quite noisy due to the presence of mechanical equipment.

MODAL IDENTIFICATION

FOUR-STORY BUILDING

The modal periods and modeshapes which were identified in the north-south direction are presented in **Table 1-1** and **Table 1-2**. **Figure 1-3** shows the correlated data and corresponding power spectrum from one of these vibration tests. The fundamental north-south flexural mode is clearly evident at a period of 0.40 seconds (2.5 Hz natural frequency), while the first torsional mode (0.28 second period or 3.6 Hz frequency) and the second flexural (0.14 second period or 7 Hz frequency) also have detectable contributions.

The modal information from the east-west tests is in **Table 1-3** and **Table 1-4**, while a representative correlation function and power spectrum are shown in **Figure 1-4**. The first east-west flexural modal period is 0.41 seconds (frequency of 2.4 Hz). The second peak in the power spectrum is close to the frequency of the first north-south mode, so perhaps the modeshape of this mode has a significant north-south component as well. The second east-west flexural mode is probably at a period of 0.15 seconds (frequency of 6.7 Hz). The results from the second flexural mode are not considered very reliable, since the response was barely above the noise level in the power spectrum and the extracted frequency and damping parameters varied significantly from each test. The modeshape components MODE-ID was able to identify did resemble a second flexural mode.

Figure 1-5, **Figure 1-6**, and **Figure 1-7** depict the modeshapes for the first north-south flexural mode, the first east-west flexural mode, and the second north-south flexural mode, respectively.

The rocking and torsional components which were identified from the tests at the foundation were quite small and were considered negligible. It was concluded that soil-structure interaction was not important in the building's dynamic behavior, at least at the low amplitude levels of the AVS.

ADJACENT TWO-STORY BUILDING

The modal parameters from the two-story building were difficult to identify, as seen by the relatively small peaks in the power spectrum of the response shown in **Figure 1-8**. The fundamental-mode peak at 2.4 Hz (0.41 second period) was readily identifiable, while the parameters from the higher modes which were found were more difficult to extract consistently, see **Table 1-5** and **Table 1-6**. The identified modeshapes are three-dimensional but are not consistent with expectations and are deemed unreliable due to the poor signal-to-noise ratio of the signals.

DISCUSSION

The ambient vibration survey was successful in identifying the lower modes of the small-amplitude vibrations of the four-story building, but had less success for the two-story building where the modal contributions were not well expressed in the recorded AVS signals. Although the natural periods for the four-story building did not compare very well with those from the analytical model, the ratios of corresponding observed and model periods were consistently similar, giving a period ratio of about 0.4, as shown in **Table 1-1** and **Table 1-3**. Prior studies suggest a possible explanation of this result, as discussed in the Conclusions section of this report.

WEST LA BUILDING (TASK 3.1 BUILDING 6)

The second set of field tests were performed on an eleven-story steel-frame structure located in West LA. The moment connections in this building suffered a significant number of failures during the Northridge Earthquake, and have not yet been repaired. The tests were performed from 9:00 A.M. until 5:00 P.M. on March 3rd. The weather was partly cloudy, with calm winds ($\leq$ 10 mph). The building was uninhabited, except for the test crew and some maintenance and security personnel.

BUILDING DESCRIPTION

The eleven-story steel-frame building is somewhat irregular in shape, and has no uniform floor plan. A rectangular parking structure surrounding an elevator core comprises the bottom five levels, with a typical floor plan shown in **Figure 1-9** (the beams indicated in bold in the figure, and the associated columns, comprise the moment frame). The top six stories are all offices, and the floor plan for these levels steps back from one column line in the plan to the next to form a series of terraces on the building's exterior. The locations of the stairwells are indicated in the drawing by the large ⊠ at either end of the building. The landings of the stairs served as the location for the seismometers during the tests so the instruments could be placed at the same location in the floor plan for each level. The building has no basement level.

F. Naeim of John A. Martin & Associates provided a table of modal periods derived from an ETABS model of the structure. The first twelve of these appear in **Table 1-7**.

SENSOR CONFIGURATIONS

In order to obtain three-dimensional modeshape information, north and west measurements were taken at each sensor location. The two reference channels (Ranger 3 facing north and Ranger 4 facing west) were located near the elevators in the center of the eleventh floor and remained there for all of the tests. Rangers 1 (north) and 2 (west) were placed in the north-west stairwell and Rangers 5 (north) and 6 (west) in the south-east stairwell. Rangers 1,2,5, and 6 were initially located on the eleventh floor and were moved down one floor following each series of tests. The sensor locations are labeled with an '×' in **Figure 1-9**. The channel numbers referenced in the text and figures correspond to these sensor numbers.

Four sets of data were recorded for 180 seconds at 500 Hz with the sensors at each of the top six floors, then three sets of data were recorded for the same duration on the fifth through first floors. A final set of tests was run (three sets of 180 seconds each at 500 Hz) with the sensors oriented vertically on the ground floor to capture the rocking components of the modeshapes.

DATA PROCESSING

Again, the data processing was performed at Caltech. Some care was required to extract the modal parameters due to the three-dimensional modeshapes as well as the closely spaced natural periods. Instead of choosing a reference channel facing north or west, a reference channel facing north-west (obtained from a linear combination of the measured channels) was found to contain large enough components of all the modes to provide consistent results.

The ambient vibration data from the eleven-story building proved to be quite rich in modal information. From some of the tests, up to nine potential modes could be identified using MODE-ID. The raw data from one of the tests with the seismometers on the tenth floor (and the two reference ones on the eleventh) is shown in **Figure 1-10**. The sample correlation function and power spectrum are displayed for channels 1 and 2 in **Figure 1-11**. To determine which of the peaks in the power spectrum were actual structural modes, the modeshape components for each possible natural frequency were computed at as many floors as possible. Comparison of these values from one test run to the next as well as visualization of the overall modeshapes helped to determine which were actual structural modes.

The theoretical correlation function, calculated based on the modal parameters which were identified with MODE-ID, was shown to closely resemble the sample correlation. In **Figure 1-12**, the theoretical and sample correlations are plotted together for each channel, and they are nearly coincident (often indistinguishable), demonstrating a good fit of the linear model to the data.

MODAL IDENTIFICATION

The six modes identified with a high degree of confidence are listed in **Table 1-8**. This table also shows the ratio of the identified and model periods. The mode descriptions given in the figures and tables (e.g. 1^{st} north-south) reflect the dominant motion of the mode. The north-south modes were found to be predominantly north-south while the east-west modes possessed a significant torsional component.

The modeshapes for the first six modes of vibration are plotted in **Figure 1-13** through **Figure 1-18**. Their values are listed in **Table 1-10** through **Table 1-15**. Note that in these plots only the first 10 stories are depicted since obstacles such as an elevated heliport prevented roof measurements from being taken. Additionally, the rectangular shape of each floor plan does not reflect the actual plan, which varies with height, but is drawn to enclose the sensors located at opposite corners of the building.

The modeshape components identified from the eleventh floor data sets show the motion of the north facing reference channel (located near the center of the floor) being 1.5 times larger

than that for either of the other two north facing channels. This implies some bowing in the first mode on that floor. Since the center motion is measured only on the eleventh floor, this result is not presented as part of the identified modeshapes plotted in the figures.

Three higher modes with periods between 0.19 and 0.21 seconds were identified with less confidence. The modal periods were found consistently, but the three-dimensional modeshapes, closely spaced natural periods, and small amplitudes of these modes made identification of their modeshapes difficult. These modes are believed to correspond to the three model modes with periods between 0.29 and 0.32 seconds because the ratios of identified periods to the model periods (shown in **Table 1-9**) agree with the ratios found for the lower modes.

Some other possible modes with periods of 0.24, 0.29 and 0.30 seconds were identified. The validity of these modes is in question for two reasons. First, they could only be identified from data taken on floors seven through eleven. Additionally, these modes were only identified from some of the tests taken on these floors.

From analysis of the tests to measure the building's rocking on its foundation, the rocking components were found to be small and were deemed insignificant.

DISCUSSION

The ambient vibration survey conducted on Building 6 of Task 3 was successful in identifying the structure's first six modes of vibration, and possibly some others. For the first four translational modes, the ratios of the AVS modal periods to those from the analytical model of F. Naeim were all about 0.67, while the corresponding period ratios for the first two torsional modes were 0.76 and 0.82 respectively (see **Table 1-8**). Finding which of the higher modes in the model corresponded to the modes identified from the tests was more difficult; particularly since no model modeshape information was available for comparison.

As in the Northridge buildings, the modal periods from the ambient vibration survey were significantly lower than those obtained from the analytical model, indicating that the actual structure has more stiffness for low-amplitude vibrations than was modeled. Possible reasons for this behavior are discussed in the Conclusions section of this report.

CONCLUSIONS

We were successful in identifying the modal parameters for the lower modes of vibration from the ambient vibration surveys conducted on one four-story and one eleven-story steel-frame building. The identified modal periods were compared with those from analytical models of the two buildings prepared under SAC Task 3.1 and found to be shorter.

An explanation for the difference in periods is that the models considered only the structural frame in the stiffness calculation. At low levels of vibration, such as in an AVS, non-structural elements like architectural partitions or building cladding can contribute significantly to the stiffness, thus shortening the natural periods. As vibration amplitudes increase, the effective stiffness decreases due to loosening or slipping of non-structural components, thereby increasing the natural periods of the building. Therefore, as the excitation level increases, the observed periods approach the periods computed from an analytical model treating only the structural system. This behavior is consistent with limited past studies (Beck, 1978; McVerry, 1979) which showed that the identified periods from seismic response were closer to the model periods than to the identified AVS periods.

The ratios between AVS and analytical model modal periods obtained in this study were similar for nearly all identified structural modes of a building, although they were different for each building. Assuming that measured seismic periods approximately reflect the model periods, prior studies corroborate this result. For example, a study of five buildings in the San Francisco Bay area indicated that the ratio of periods for different modes from ambient and strong motion vibration records may be characteristic of a given building(Phan et al., 1992). Another study (McVerry, 1979) demonstrated this result for a number of buildings in the Los Angeles area. The period ratio does change from building to building, but no studies have been found which investigate how differences in the design and construction, or damage to the building, affect it.

Recent testing of the Millikan Library building on the campus of the California Institute of Technology used an eccentric mass shaker to excite the structure. For low excitation levels, the natural periods found were similar to those determined during a previous AVS (Beck et al., 1994a). With increased excitation levels, the periods of the first north-south, east-west, and torsional modes increased. Preliminary analysis of the data suggests that for a given excitation level, the ratios of corresponding AVS and forced vibration periods for each of the identified modes are similar. This implies that the excitation level as well as the building characteristics affect the period ratios.

The period-ratio data imply that the lower mode periods of a building scale uniformly with changing response amplitude. This behavior could be caused by a nearly constant proportional decrease in stiffness over the building as the response level increases. A nearly uniform shedding of nonstructural stiffness would provide such a change in stiffness.

This study has shown that a considerable amount of modal information can be identified using ambient vibration data. Further work will be needed in order to show the usefulness of ambient vibration surveys in model validation and health monitoring.

FUTURE WORK

We strongly recommend two further projects. The first would consist of further AVS of steel-frame buildings damaged in the Northridge earthquake and re-testing of damaged buildings, such as the eleven-story one described in this report, after they have been repaired. These "before" and "after" tests could then form a very valuable database against which to test proposed global damage detection methodologies based on ambient vibrations. An example of such a procedure is the two-stage approach involving an AVS and model updating developed by J. Beck (Beck et al., 1994b).

The second suggested project would entail using Northridge Earthquake (or other earthquake) response records from steel-frame buildings to identify modal properties under much larger levels of excitation. Comparison of these results with those from analytical models and ambient vibration surveys for the same buildings would enhance our understanding of how to reconcile the modal parameters identified through the various methods. Since an AVS can be done efficiently, cheaply and unobtrusively, this knowledge is important in determining the utility of these surveys in assessment of models used in earthquake-resistant design.

ACKNOWLEDGEMENTS

The authors wish to acknowledge the assistance of Farzad Naeim and Charles Thiel in gaining access to the West LA and CSUN buildings respectively. We appreciate the valuable assistance of Raul Relles during the field testing. We also are thankful to the Albert Niu Lin Laboratory of Structural Dynamics at Caltech for lending us the test equipment used in this study.

Table 1-1: Modal periods, north-south direction, CSUN 4-story building.

Mode Description	AVS Period	Model Period	Ratio AVS/Model
First flexural	0.40	1.07	0.37
First torsional	0.28	0.68	0.41
Second flexural	0.14	0.36	0.39

NOTE : The model periods were supplied by H. Krawinkler and C. Thiel.

Table 1-2: Modeshape components, north-south direction, CSUN 4-story building.

Location	Modeshape Component		
	1^{st} flexural	1^{st} torsional	2^{nd} flexural
floor 2, NW	0.13	0.11	0.23
floor 3, NW	0.29	0.17	0.38
floor 4, NW	0.60	0.22	0.04
roof, NW	0.62	0.13	-0.50
roof, SE	0.40	-0.92	-0.74

NOTES

1. The 6^{th} channel was in a noisy location, so its results may be inaccurate.
2. The Ranger in the southeast corner on the third floor was not functioning in this test

Table 1-3: Modal periods, east-west direction, CSUN 4-story building.

Mode Description	AVS Period	Model Period	Ratio AVS/Model
First flexural	0.41	1.05	0.39
Second flexural	0.15	0.36	0.41

NOTE : The estimation of the 2nd flexural mode should be considered suspect, since its relative amplitude was quite small.

Table 1-4: Modeshape components, east-west direction, CSUN 4-story building.

Location	Modeshape Component	
	Mode 1	Mode 2
floor 2, NW	0.08	0.26
floor 3, NW	0.18	0.37
floor 3, SE	0.18	0.39
floor 4, NW	0.43	0.19
roof, NW	0.46	-0.31
roof, SE	0.73	-0.70

NOTE : The 6^{th} channel was in a noisy location, so its results may be inaccurate.

Table 1-5: Modal periods, CSUN 2-story building.

Mode Description	AVS Period	Model Period
First mode	0.41	n/a
Second mode	0.28	n/a
Third mode	0.23	n/a

NOTES

1. No accompanying analytical model was available.
2. The results from the second and third modes are rather suspect, since their contribution to the overall response is quite small.

Table 1-6: Modeshape components, CSUN 2-story building.

Sensor Information		Modeshape Component		
Location	Direction	Mode 1	Mode 2	Mode 3
floor 2, SE	W	0.30	0.09	-0.06
floor 2, SE	N	-0.25	0.22	0.28
floor 2, NE	W	-0.05	0.55	0.10
roof, SE	W	0.77	0.30	-0.13
roof, SE	N	-0.02	0.50	0.05
roof, NE	W	-0.43	0.50	0.93

NOTE : The 6^{th} channel was again located near noisy machinery, so its results may be inaccurate.

Table 1-7: First twelve model periods, 11-story building

Mode	Period (sec)	Mode	Period (sec)
1	1.81	7	0.46
2	1.69	8	0.43
3	1.10	9	0.32
4	0.79	10	0.30
5	0.72	11	0.29
6	0.50	12	0.24

NOTE : These results are from F. Naeim of John A. Martin & Associates.

Table 1-8: First six identified periods, 11-story building

Mode Description	AVS Period	Ratio AVS/Model
1^{st} NS mode	1.20	0.67
1^{st} EW mode	1.14	0.67
1^{st} Torsion mode	0.83	0.76
2^{nd} NS mode	0.53	0.67
2^{nd} EW mode	0.48	0.66
2^{nd} Torsion mode	0.41	0.82

NOTE : The ratios presented assume that the first six identified modes correspond to the first six model modes.

Table 1-9: Other identified periods, 11-story building

Mode Description	AVS Period	Ratio AVS/Model
n/a	0.21	0.68
n/a	0.20	0.66
n/a	0.19	0.66

NOTE : The ratios presented assume that the three identified modes correspond to the ninth, tenth and eleventh model modes respectively.

Table 1-10: Modeshape components, 1^{st} N-S mode, 11-story building

Sensor location	North-West		South-East	
Sensor orientation	North	West	North	West
	Modeshape component			
Floor 11	1.20	0.02	1.76	-0.52
Floor 10	1.03	0.03	1.60	-0.43
Floor 9	0.94	0.03	1.39	-0.32
Floor 8	0.76	-0.03	1.15	-0.21
Floor 7	0.54	0.06	0.89	-0.11
Floor 6	0.44	0.01	0.69	0.03
Floor 5	0.33	0.05	0.51	0.00
Floor 4	0.28	0.05	0.41	-0.03
Floor 3	0.11	0.03	0.31	0.03
Floor 2	0.05	0.00	0.12	-0.02
Floor 1	0.00	0.00	0.03	0.00

Table 1-11: Modeshape components, 1^{st} E-W mode, 11-story building

Sensor location	North-West		South-East	
Sensor orientation	North	West	North	West
	Modeshape component			
Floor 11	0.33	0.80	-0.11	1.71
Floor 10	0.22	0.70	-0.10	1.46
Floor 9	0.17	0.58	-0.07	1.31
Floor 8	-0.06	0.55	-0.11	1.20
Floor 7	0.11	0.37	0.04	0.90
Floor 6	0.14	0.30	-0.08	0.49
Floor 5	0.04	0.19	-0.11	0.40
Floor 4	0.13	0.15	-0.08	0.39
Floor 3	0.02	0.07	-0.07	0.28
Floor 2	0.01	0.02	0.01	0.08
Floor 1	0.00	0.00	-0.00	0.01

Table 1-12: Modeshape components, 1^{st} torsion mode, 11-story building

Sensor location	North-West		South-East	
Sensor orientation	North	West	North	West
	Modeshape component			
Floor 11	-1.88	1.36	1.67	-0.18
Floor 10	-1.66	0.84	1.62	-0.16
Floor 9	-1.42	0.98	1.37	0.07
Floor 8	-0.73	0.69	1.00	-0.18
Floor 7	-0.73	0.49	0.87	-0.21
Floor 6	-0.56	0.31	0.63	-0.32
Floor 5	-0.44	0.23	0.56	-0.26
Floor 4	-0.42	0.20	0.44	-0.25
Floor 3	-0.25	0.04	0.32	-0.19
Floor 2	-0.07	0.04	0.13	-0.08
Floor 1	-0.01	-0.03	0.02	-0.02

Table 1-13: Modeshape components, 2^{nd} N-S mode, 11-story building

Sensor location	North-West		South-East	
Sensor orientation	North	West	North	West
	Modeshape component			
Floor 11	1.1	-0.03	1.33	-0.22
Floor 10	0.1	0.04	0.51	0.06
Floor 9	-0.4	0.02	-0.32	0.08
Floor 8	-1.0	0.08	-1.00	0.13
Floor 7	-1.2	0.09	-1.29	0.18
Floor 6	-1.4	0.13	-1.68	0.26
Floor 5	-1.5	0.09	-1.42	0.09
Floor 4	-1.0	-0.03	-1.18	0.03
Floor 3	-0.8	-0.05	-0.93	0.03
Floor 2	-0.3	-0.07	-0.42	-0.02
Floor 1	0.0	-0.10	-0.04	0.00

Table 1-14: Modeshape components, 2^{nd} E-W mode, 11-story building

Sensor location	North-West		South-East	
Sensor orientation	North	West	North	West
	Modeshape component			
Floor 11	1.30	0.70	-0.91	2.21
Floor 10	0.95	0.17	-0.68	1.12
Floor 9	0.08	-0.45	0.07	-0.39
Floor 8	-0.20	-1.08	0.35	-1.60
Floor 7	-0.63	-1.74	0.59	-2.70
Floor 6	-0.80	-1.68	0.68	-3.20
Floor 4	-0.91	-0.97	0.85	-2.24
Floor 3	-0.26	-0.66	0.49	-1.57

Table 1-15: Modeshape components, 2^{nd} torsion mode, 11-story building

Sensor location	North-West		South-East	
Sensor orientation	North	West	North	West
	Modeshape component			
Floor 11	-1.91	1.53	1.32	0.15
Floor 10	-1.19	0.73	0.71	0.04
Floor 9	0.01	-0.36	-0.12	-0.23
Floor 8	1.04	-1.14	-0.63	-0.59
Floor 7	1.67	-1.88	-1.12	-0.64
Floor 6	1.56	-1.97	-1.31	-0.75
Floor 5	1.78	-1.88	-1.34	-0.66
Floor 4	1.21	-1.30	-1.00	-0.44
Floor 3	1.18	-0.94	-0.78	-0.31
Floor 2	0.41	-0.44	-0.25	-0.13
Floor 1	0.02	-0.03	0.00	0.08

Figure 1-1: Typical floor plan, CSUN 4-story building.

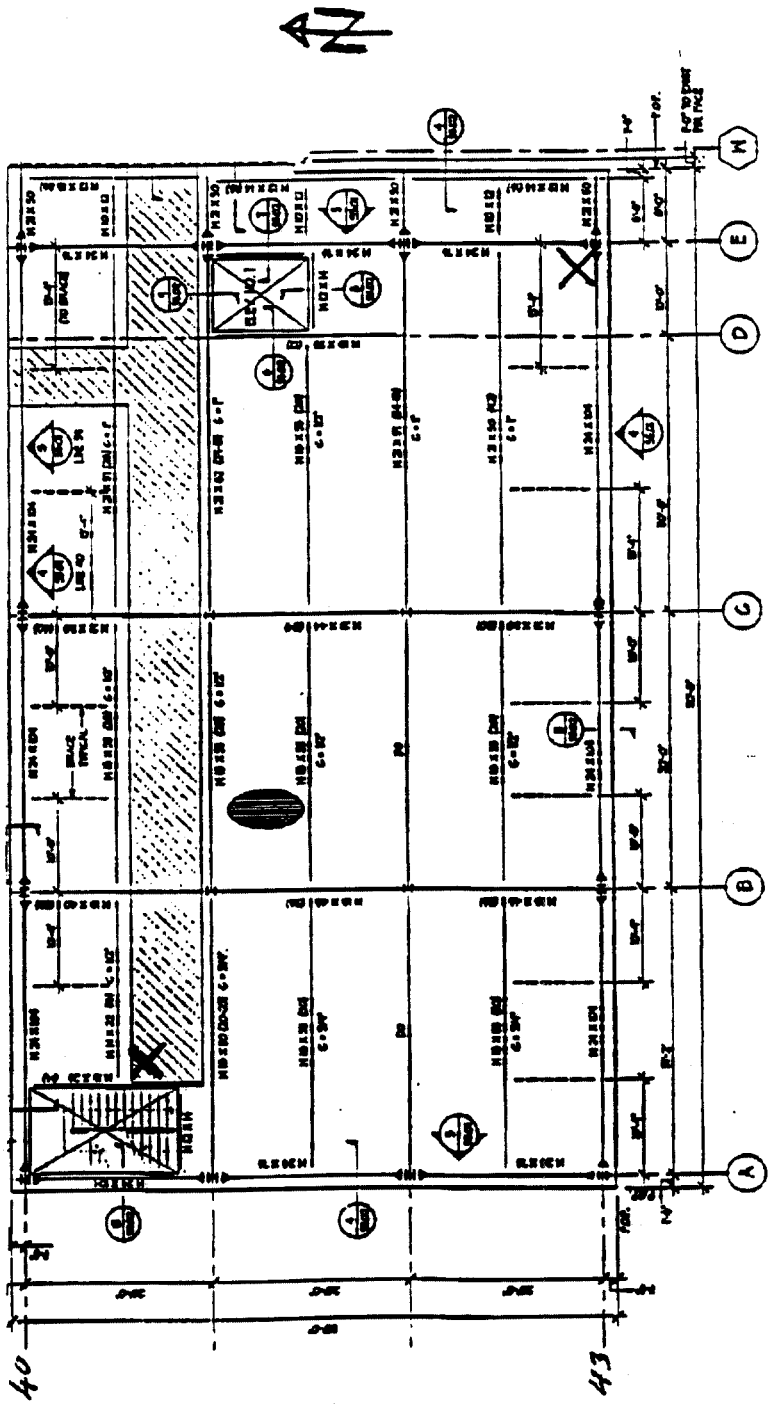

Figure 1-2: Sensor locations, CSUN 2-story building.

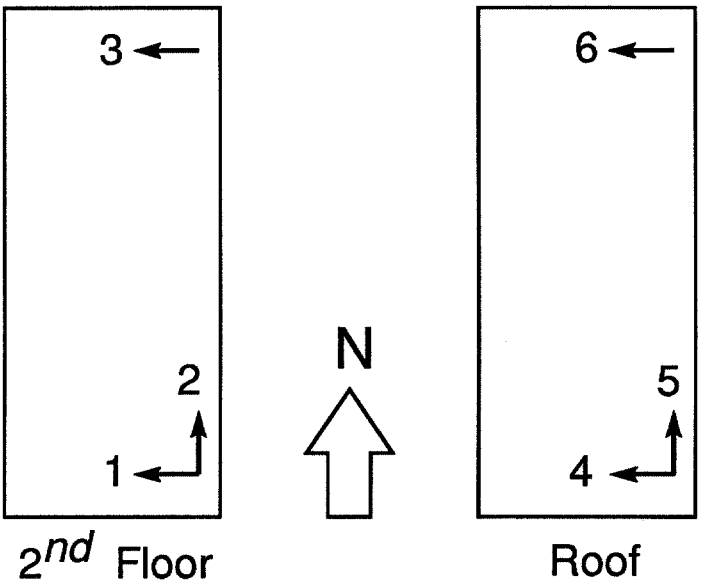

Figure 1-3: Signals from north-south tests, CSUN 4-story building.

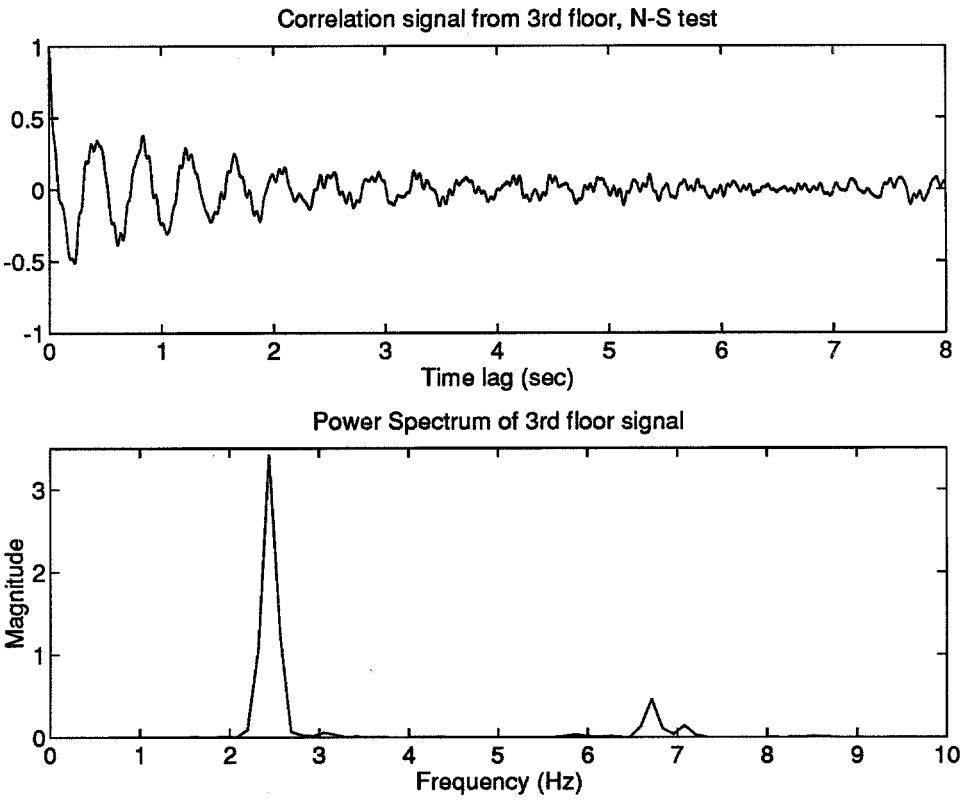

Figure 1-4: Signals from east-west tests, CSUN 4-story building.

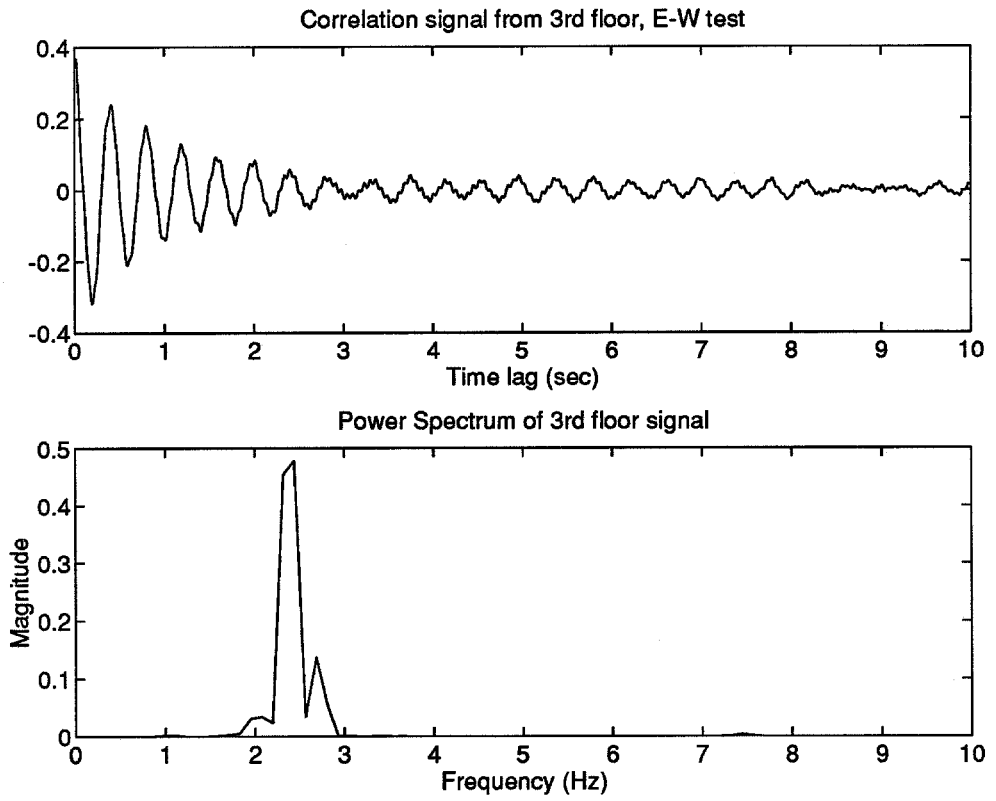

Figure 1-5: First north-south mode, 4-story building.

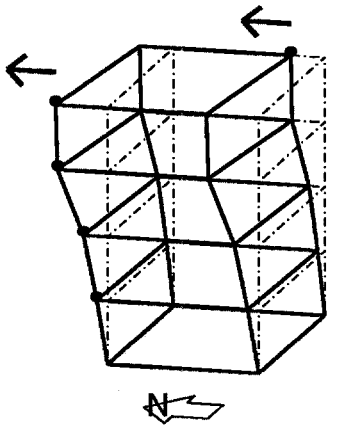

NOTE : The dots represent sensor locations and the arrows denote their orientation.

Figure 1-6: First east-west mode, 4-story building.

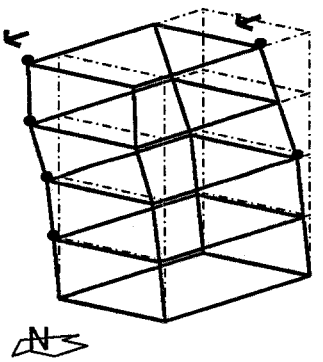

Figure 1-7: Second north-south mode, 4-story building.

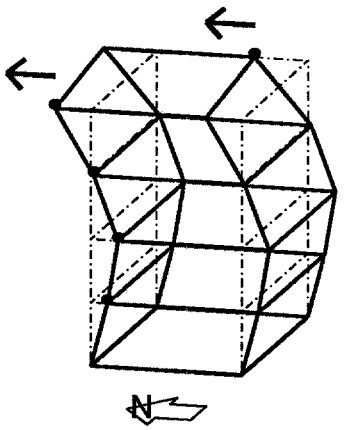

Figure 1-8: Signals from tests on CSUN 2-story building.

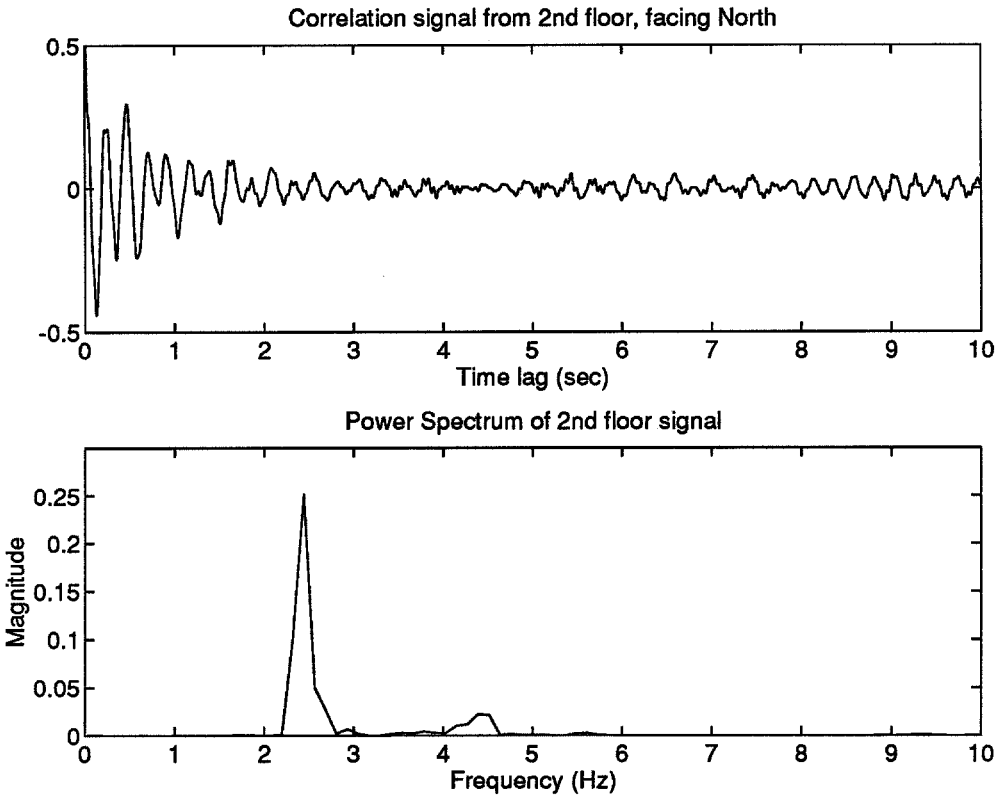

Figure 1-9: "Typical" floor plan for the 11-story building.

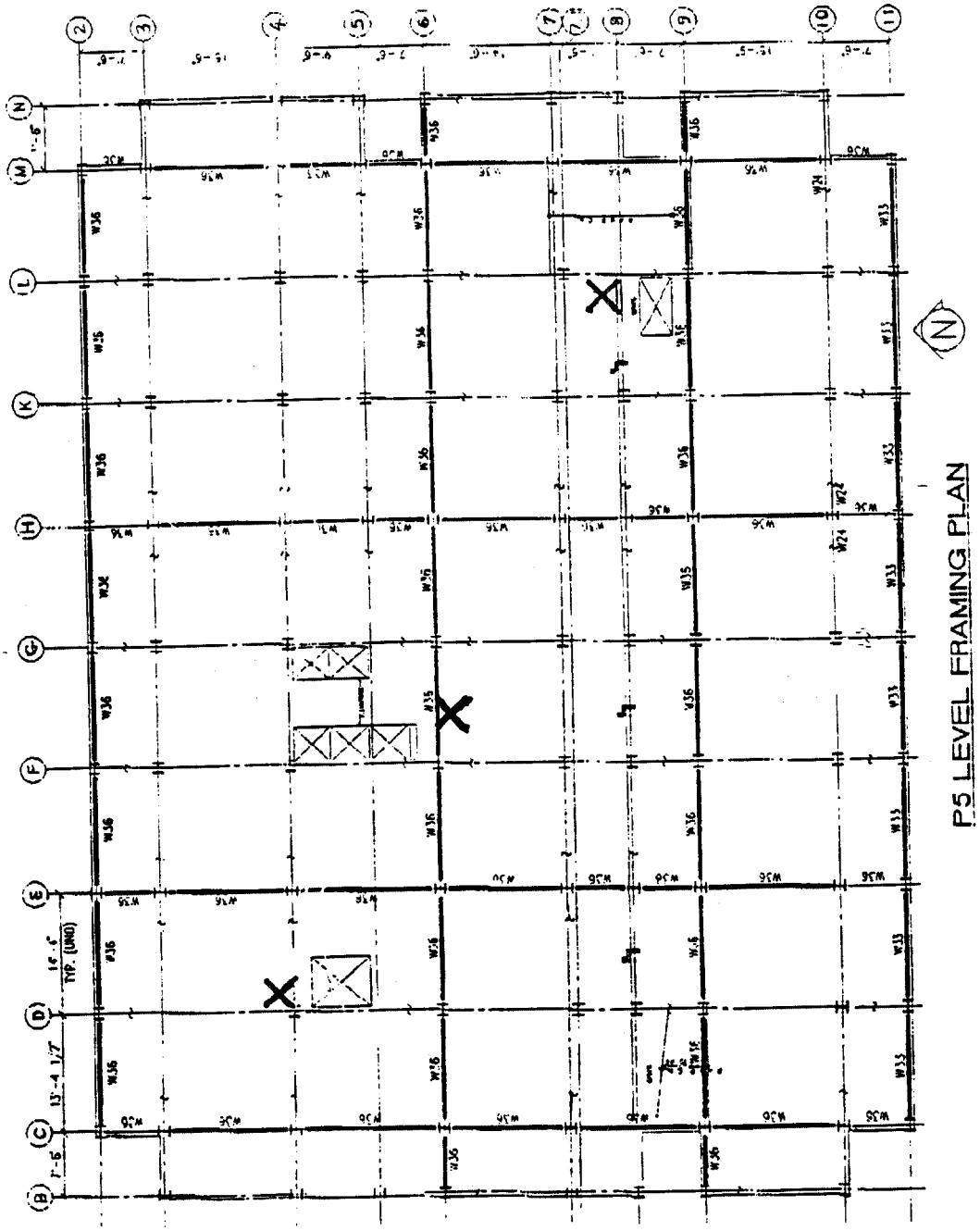

Figure 1-10: Raw signals from 10^{th} floor test, 11-story building.

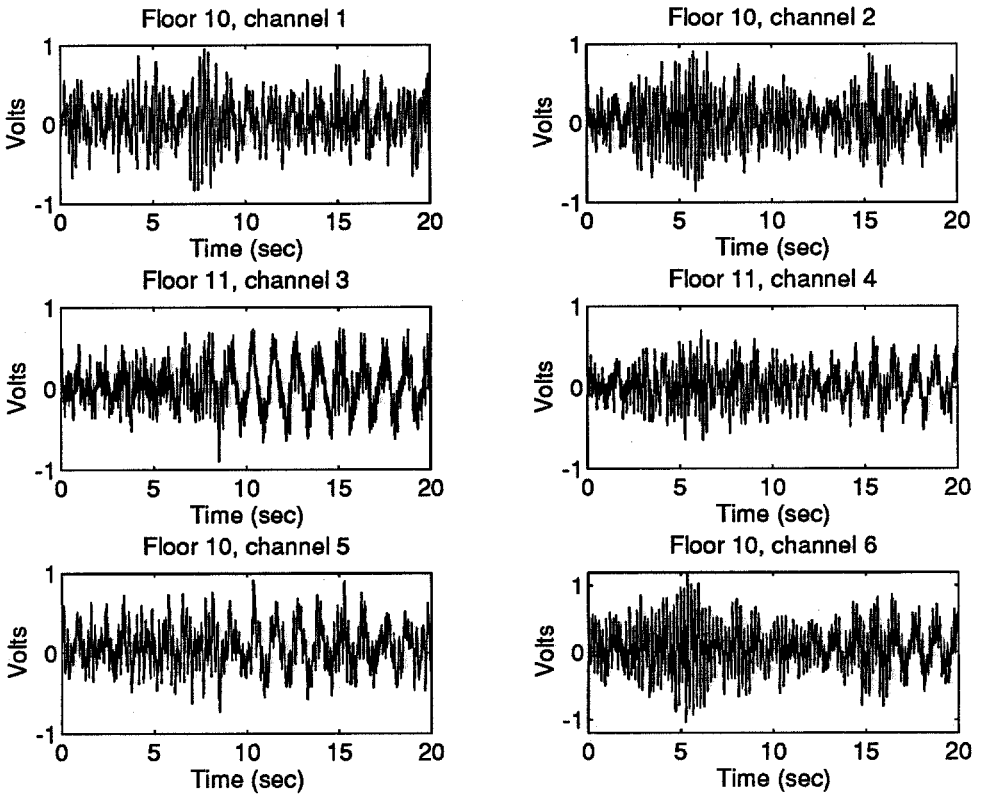

Figure 1-11: Correlation function and power spectrum, 10^{th} floor of 11-story building.

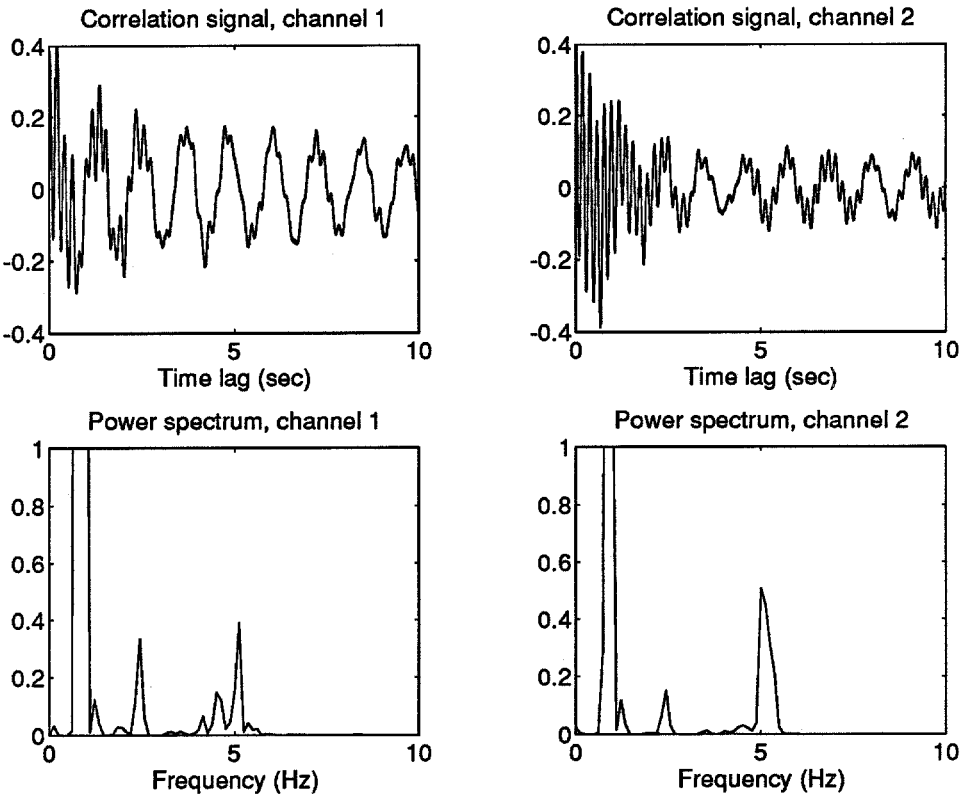

Figure 1-12: Comparison between sample and theoretical correlation.

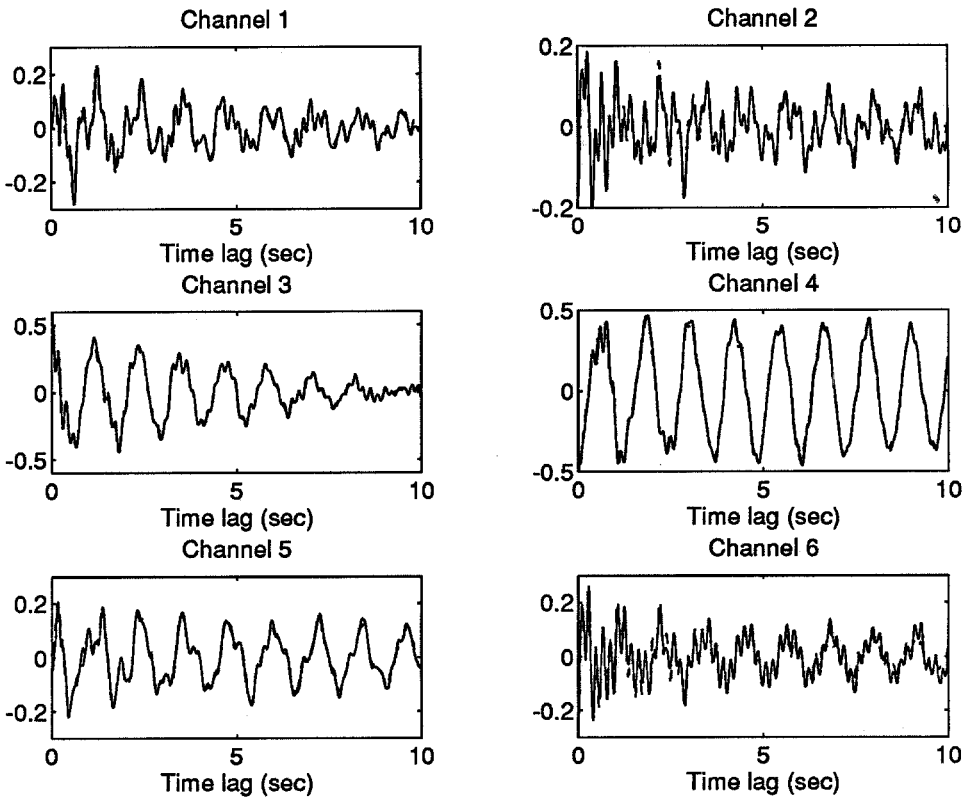

NOTES

1. The results are from a 6^{th} floor test.

2. The dashed line is the theoretical correlation function obtained from the identified modal parameters, while the solid line is the sample correlation.

Figure 1-13: First north-south mode, 11-story building.

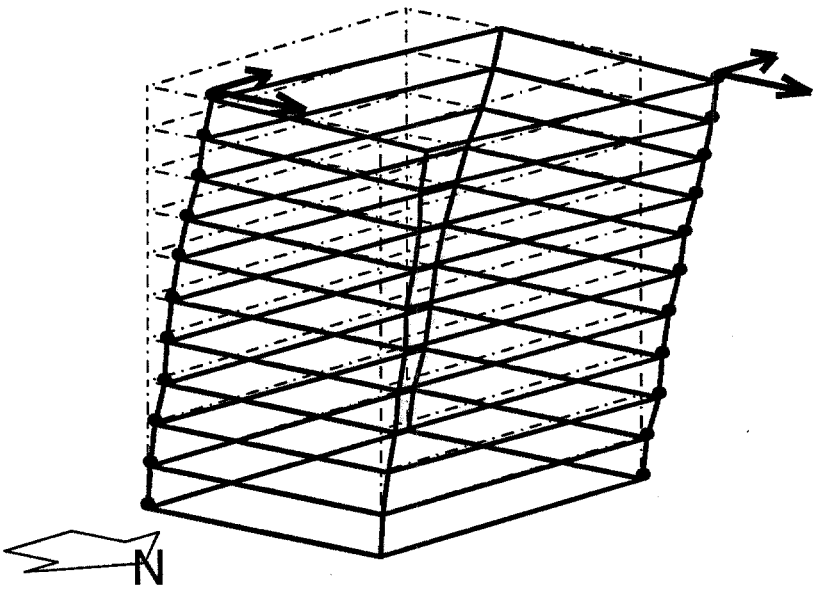

NOTES

1. For simplicity, the modeshapes are depicted for a structure with a constant rectangular plan.

2. The dots represent sensor locations and the arrows denote their orientation.

Figure 1-14: First east-west mode, 11-story building.

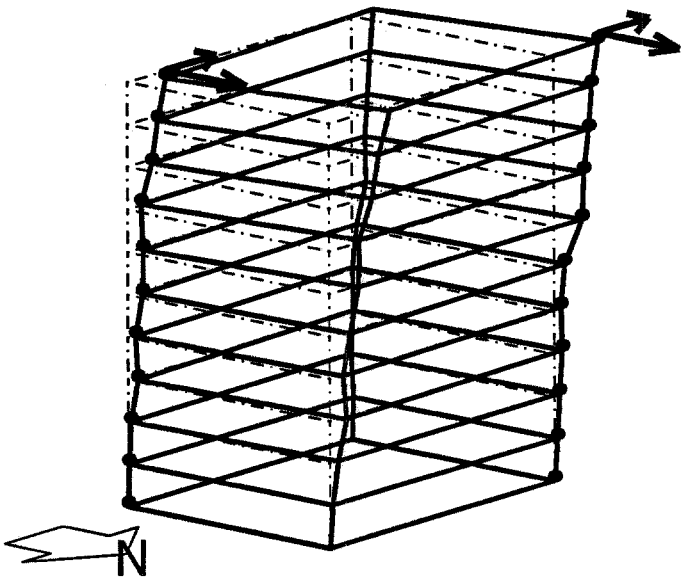

Figure 1-15: First torsional mode, 11-story building.

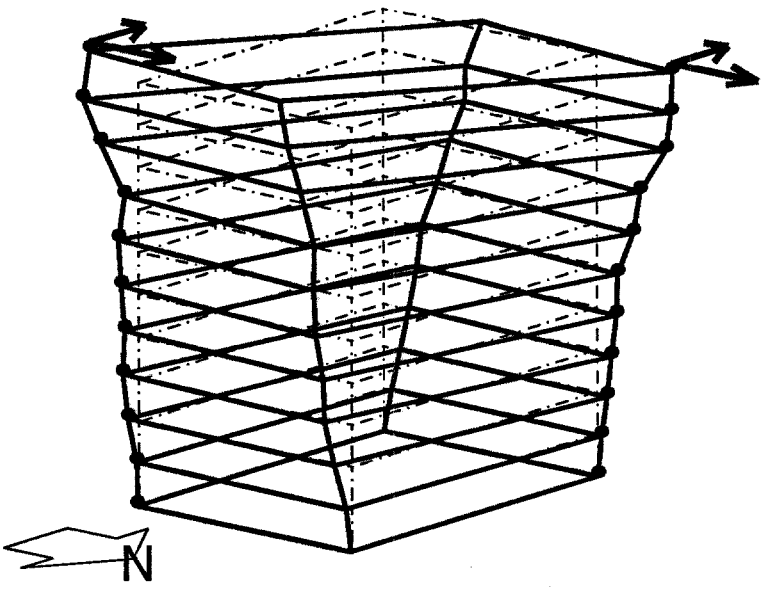

Figure 1-16: Second north-south mode, 11-story building.

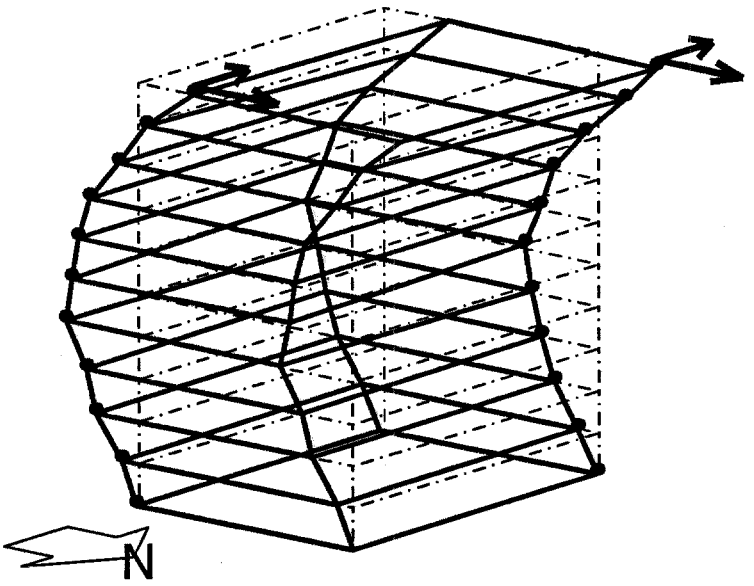

Figure 1-17: Second east-west mode, 11-story building.

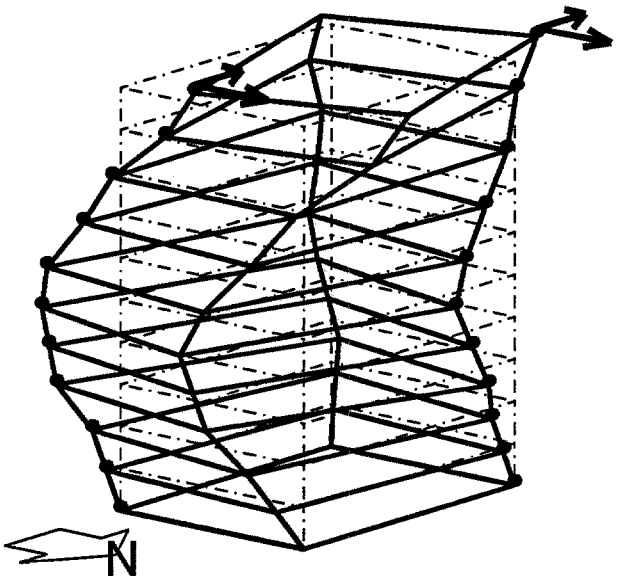

NOTE : There is a considerable amount of torsion in this mode.

Figure 1-18: Second torsional mode, 11-story building.

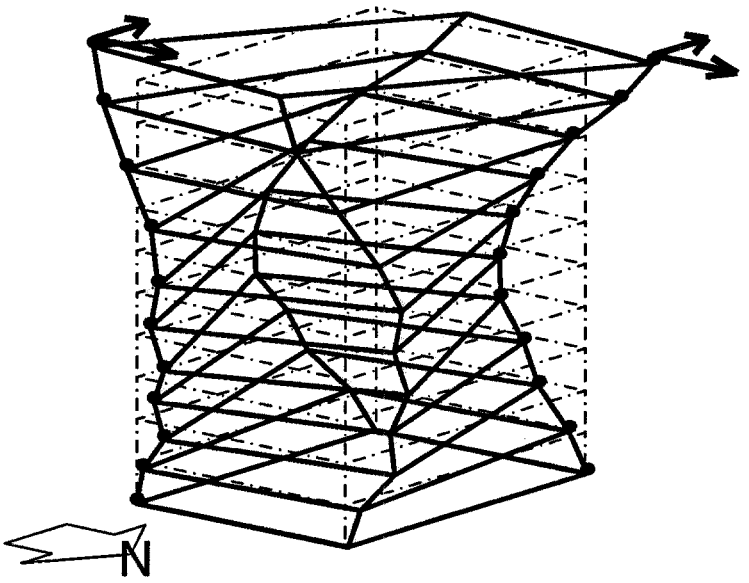

References

Beck, J. L. (1978). Determining models of structures from earthquake records. Technical Report EERL78-01, California Institute of Technology.

Beck, J. L. (1989). Statistical system identification of structures. In *Fifth International Conference on Structural Safety and Reliability*, pages 1395–1402, New York. ASCE.

Beck, J. L. and Jennings, P. C. (1980). Structural identification using linear models and earthquake records. *Earthquake Engineering and Structural Dynamics*, 8:145–160.

Beck, J. L., May, B. S., and Polidori, D. C. (1994a). Determination of modal parameters from ambient vibration data for structural health monitoring. In *Proceedings First World Conference on Structural Control*, pages TA3:3–12, Pasadena, California.

Beck, J. L., Vanik, M. W., and Katafygiotis, L. S. (1994b). Determination of stiffness changes from modal parameter changes for structural health monitoring. In *Proceedings First World Conference on Structural Control*, pages TA3:13–22, Pasadena, California.

Beck, R. T. and Beck, J. L. (1985). Comparison between transfer function and modal minimization method for system identification. Technical Report EERL85-06, California Institute of Technology.

Bendat, J. S. and Piersol, A. G. (1980). *Engineering Applications of Correlation and Spectral Analysis*. John Wiley & Sons.

Caughey, T. K. and O'Kelly, M. E. J. (1965). Classical normal modes in damped linear dynamic systems. *ASCE J. of Applied Mechanics*, 32:583–588.

James, G. H., Carne, T. G., and Lauffer, J. P. (1992). The natural excitation technique for modal parameter extraction from operating wind turbines. Technical Report SAND92-1666 • UC-261, Sandia National Laboratories.

Mason, A. B., Beck, J. L., Chen, J. C., and Ullmann, R. R. (1989). Modal parameter identification of an offshore platform from earthquake response records. In *Proceedings Sessions Related to Seismic Engineering at Structures Congress*, pages 217–226. ASCE.

McVerry, G. H. (1979). Frequency domain identification of structural models from earthquake records. Technical Report EERL79-02, California Institute of Technology.

Nisar, A. D., Werner, S. D., and Beck, J. L. (1992). Assessment of UBC seismic design provisions using recorded building motions. In *Proceedings Tenth World Conference on Earthquake Engineering*, pages 5723–5728, Balkema, Rotterdam.

Phan, L. T., Marshal, R. D., and Celebi, M. (1992). Response of buildings to ambient vibration and the Loma Prieta earthquake: A comparison. In *Proceedings Tenth Structures Congress*, pages 583–586, San Antonio, Texas.

Werner, S. D., Beck, J. L., and Levine, M. B. (1987). Seismic response evaluation of Meloland Road Overpass using 1979 Imperial Valley earthquake records. *Int. J. Earthquake Engineering and Structrual Dynamics*, 15:249–274.